On the fixed-stress split scheme as smoother in multigrid methods for coupling flow and geomechanics

Francisco J. Gaspar[a], Carmen Rodrigo[b,*]

[a] *CWI, Centrum Wiskunde & Informatica, Science Park 123, P.O. Box 94079, 1090 Amsterdam, The Netherlands*
[b] *IUMA and Department of Applied Mathematics, University of Zaragoza, María de Luna, 3, 50018 Zaragoza, Spain*

Abstract

The fixed-stress split method has been widely used as solution method in the coupling of flow and geomechanics. In this work, we analyze the behaviour of an inexact version of this algorithm as smoother within a geometric multigrid method, in order to obtain an efficient monolithic solver for the Biot's problem. This solver combines the advantages of being a fully coupled method, with the benefit of decoupling the flow and the mechanics part in the smoothing algorithm. Moreover, the fixed-stress split smoother is based on the physics of the problem, and therefore all parameters involved in the relaxation are based on the physical properties of the medium and are given a priori. A local Fourier analysis is applied to study the convergence of the multigrid method and to support the good convergence results obtained. The proposed geometric multigrid algorithm is used to solve several tests in semi-structured triangular grids, in order to show the good behaviour of the method and its practical utility.

Keywords: Iterative Fixed-stress split scheme, Smoother, Multigrid, Poroelasticity, Local Fourier Analysis

2010 MSC: 00-01, 99-00

*Corresponding author.
Email addresses: F.J.Gaspar@cwi.nl (Francisco J. Gaspar), carmenr@unizar.es (Carmen Rodrigo)

1. Introduction

In recent years, intensive research has been focused on the design of efficient methods for solving the large linear systems arising from the discretization of the Biot's model, since in real simulations it is the most consuming part. Using an implicit time-stepping discretization, the resulting system matrix on each time step is an example of saddle point problem requiring therefore specific solvers. There are mainly two approaches, the so-called monolithic or fully coupled methods and the iterative coupling methods. In the monolithic approach, the linear system is solved simultaneously for all the unknowns, and it usually provides unconditional stability and convergence. The challenge here, is the design of efficient preconditioners to accelerate the convergence of Krylov subspace methods and the design of efficient smoothers in a multigrid framework. Recent advances in both directions can be found in [1, 2, 3, 4] and the references therein. On the other hand, at each time step, iterative coupling methods solve sequentially the equations for fluid flow and geomechanics, until a converged solution within a prescribed tolerance is achieved. A big advantage of these methods is their flexibility since two different codes for fluid flow and geomechanics can be linked for solving the poroelastic problems. The most used iterative coupling methods are the drained and undrained splits, which solve the mechanical problem first, and the fixed-strain and fixed-stress splits, which on the contrary solve the flow problem first [5, 6].

Due to its unconditional stability, one of the most frequently used schemes of this type is the so-called fixed-stress split method. This sequential-implicit method basically consists in solving the flow problem first fixing the volumetric mean total stress, and then the mechanics part is solved from the values obtained at the previous flow step. The unconditional stability of the fixed-stress split method is shown in [7] using a von Neumann analysis. In addition, stability and convergence of the fixed-stress split method have been rigorously established in [8]. Recently, in [9] the authors have proven the convergence of the fixed-stress split method in energy norm for heterogeneous problems. Estimates for the

case of the multirate iterative coupling scheme are obtained in [10], where multiple finer time steps for flow are taken within one coarse mechanics time step, exploiting the different time scales for the mechanics and flow problems. In [11], the convergence of this method is proven in the fully discrete case when space-time finite element methods are used. In [12], the authors present a very interesting approach which consists to re-interpret the fixed-stress split scheme as a preconditioned-Richardson iteration with a particular block-triangular preconditioning operator. In fact, the four commonly used sequential splitting methods, i.e. drained-split, undrained-split, fixed-stress and fixed-strain [5], can be seen in this way [13]. It is analyzed that a fully-implicit method outperforms the convergence rate of the sequential-implicit methods. Following this approach a family of preconditioners to accelerate the convergence of Krylov subspace methods has been recently proposed for the three-field formulation of the poromechanics problem [14].

Here, we want to propose the use of an inexact version of the fixed-stress split scheme as a smoother in a geometric multigrid framework, in order to obtain an efficient monolithic solver for the Biot's problem. This approach combines the advantages of being a fully-coupled method on the one hand with the benefit of decoupling the flow and the mechanics part in the smoothing algorithm on the other hand. Recently, another decoupled smoother, based on an inexact Uzawa method, has been successfully proposed to solve the poroelastic problem in a monolithic manner [4]. However, the key for a satisfactory performance of this smoother is the choice of a relaxation parameter in the pressure update step. The main advantage of the fixed-stress split smoother proposed here is that the parameter is established by the physics of the problem, opposite to the case of the Uzawa smoother for which the relaxation parameter has to be carefully chosen.

The rest of the paper is organized as follows. Section 2 is devoted to the description of the poroelasticity model and the considered finite element discretization. In Section 3, after a brief introduction of the fixed-stress split algorithm, we introduce the class of smoothers that we proposed based on that

method, and we analyze their relaxation properties by using a smoothing local Fourier analysis technique. In Section 4, the rest of the multigrid components that we consider are listed and a two-grid local Fourier analysis is used to study the convergence of the resulting multigrid algorithm. Also in this section, the implementation of the geometric multigrid on semi-structured grids is explained in order to extend the proposed method to problems on more complex domains. Section 5 illustrates the good convergence of the multigrid method based on the fixed-stress split smoothers through two numerical experiments, one of them considering also variable coefficients. Finally, some conclusions are drawn in Section 6.

2. Mathematical model and discretization

We begin with a small introduction about the quasi-static Biot's model for soil consolidation. For a more detailed explanation about the governing equations and the mathematical model we refer to the reader to the books by Wang [15] and Coussy [16], for instance. A stabilized P1-P1 finite element method is considered to describe the solver proposed in this work as well as to present the numerical experiments. However, our approach can be easily implemented for other finite-element and finite-volume discretizations.

2.1. Mathematical model

Let Ω be a bounded open subset of $\mathbb{R}^n$, $n \leq 3$, with regular boundary Γ. According to Biot's theory [17, 18], the consolidation process must satisfy the following system of partial differential equations:

$$\text{equilibrium equation:} \quad -\operatorname{div} \boldsymbol{\sigma}' + \alpha \nabla p = \rho \boldsymbol{g}, \quad \text{in } \Omega, \tag{1}$$

$$\text{constitutive equation:} \quad \boldsymbol{\sigma}' = 2G\varepsilon(\boldsymbol{u}) + \lambda \operatorname{div}(\boldsymbol{u})\boldsymbol{I}, \quad \text{in } \Omega, \tag{2}$$

$$\text{compatibility condition:} \quad \varepsilon(\boldsymbol{u}) = \frac{1}{2}(\nabla \boldsymbol{u} + \nabla \boldsymbol{u}^t), \quad \text{in } \Omega, \tag{3}$$

$$\text{Darcy's law:} \quad \boldsymbol{q} = -\frac{1}{\mu_f}\boldsymbol{K}\left(\nabla p - \rho_f \boldsymbol{g}\right), \quad \text{in } \Omega, \tag{4}$$

$$\text{continuity equation:} \quad \frac{\partial}{\partial t}\left(\frac{1}{M}p + \alpha \nabla \cdot \boldsymbol{u}\right) + \nabla \cdot \boldsymbol{q} = f, \quad \text{in } \Omega, \tag{5}$$

where G and λ are the Lamé coefficients, $\boldsymbol{I}$ is the identity tensor, $\boldsymbol{u}$ is the displacement vector, p is the pore pressure, $\boldsymbol{\sigma'}$ and $\boldsymbol{\epsilon}$ are the effective stress and strain tensors for the porous medium, $\boldsymbol{g}$ is the gravity vector, $\boldsymbol{q}$ is the percolation velocity of the fluid relative to the soil, μ_f is the fluid viscosity and $\boldsymbol{K}$ is the absolute permeability tensor. The bulk density ρ is related to the densities of the solid (ρ_s) and fluid (ρ_f) phases as $\rho = \phi\rho_f + (1-\phi)\rho_s$, where ϕ is the porosity. M is the Biot modulus and α is the Biot coefficient given by

$$\alpha = 1 - \frac{K_b}{K_s},$$

where K_b is the drained bulk modulus , and K_s is the bulk modulus of the solid phase.

Combining equations (1)-(5), the mathematical model can be written only in terms of the displacements of the solid matrix $\boldsymbol{u}$ and the pressure of the fluid p, giving rise to the so-called two-field formulation of the Biot's consolidation model

$$-\operatorname{div}\boldsymbol{\sigma'} + \alpha\nabla p = \rho\boldsymbol{g}, \qquad \boldsymbol{\sigma'} = 2G\,\varepsilon(\boldsymbol{u}) + \lambda\operatorname{div}(\boldsymbol{u})\boldsymbol{I}, \tag{6}$$

$$\frac{\partial}{\partial t}\left(\frac{1}{M}p + \alpha\nabla\cdot\,\boldsymbol{u}\right) - \nabla\cdot\left(\frac{1}{\mu_f}\boldsymbol{K}\left(\nabla p - \rho_f\boldsymbol{g}\right)\right) = f. \tag{7}$$

To complete the formulation of a well–posed problem we must add appropriate boundary and initial conditions. For instance,

$$\begin{aligned} p = 0, \qquad & \boldsymbol{\sigma'}\,\boldsymbol{n} &&= \boldsymbol{0}, \quad \text{on } \Gamma_t, \\ \boldsymbol{u} = \boldsymbol{0}, \qquad & \boldsymbol{K}\left(\nabla p - \rho_f\boldsymbol{g}\right)\cdot\boldsymbol{n} &&= 0, \quad \text{on } \Gamma_c, \end{aligned} \tag{8}$$

where $\boldsymbol{n}$ is the unit outward normal to the boundary and $\Gamma_t \cup \Gamma_c = \Gamma$, with Γ_t and Γ_c disjoint subsets of Γ having non null measure. For the initial time, $t = 0$, the following condition is fulfilled

$$\left(\frac{1}{M}p + \alpha\nabla\cdot\boldsymbol{u}\right)(\boldsymbol{x}, 0) = 0,\ \boldsymbol{x}\in\Omega. \tag{9}$$

2.2. Discretization

We describe the discretization of the problem by the linear finite element method. For this purpose, we introduce the variational formulation for the

two-field formulation of the Biot's model as follows: For each $t \in (0, T]$, find $(\boldsymbol{u}(t), p(t)) \in \boldsymbol{V} \times Q$ such that

$$a(\boldsymbol{u}, \boldsymbol{v}) - \alpha(p, \operatorname{div} \boldsymbol{v}) = (\rho \boldsymbol{g}, \boldsymbol{v}), \quad \forall\ \boldsymbol{v} \in \boldsymbol{V}, \tag{10}$$

$$\alpha(\operatorname{div} \partial_t \boldsymbol{u}, q) + \frac{1}{M}(\partial_t p, q) + b(p, q) = (f, q) + (\boldsymbol{K}\mu_f^{-1}\rho_f \boldsymbol{g}, \nabla q), \quad \forall\ q \in Q, \tag{11}$$

where $\boldsymbol{V} = \{\boldsymbol{u} \in (H^1(\Omega))^n \mid \boldsymbol{u}|_{\Gamma_c} = \boldsymbol{0}\}$, and $Q = \{p \in H^1(\Omega) \mid p|_{\Gamma_t} = 0\}$, with $H^1(\Omega)$ denoting the Hilbert subspace of $L_2(\Omega)$ of functions with first weak derivatives in $L_2(\Omega)$, $(\cdot, \cdot)$ is the standard inner product in the space $L_2(\Omega)$, and the bilinear forms $a(\cdot, \cdot)$ and $b(\cdot, \cdot)$ are given as

$$\begin{aligned} a(\boldsymbol{u}, \boldsymbol{v}) &= 2\int_\Omega G\varepsilon(\boldsymbol{u}) : \varepsilon(\boldsymbol{v})\, \mathrm{d}\Omega + \int_\Omega \lambda \operatorname{div} \boldsymbol{u} \operatorname{div} \boldsymbol{v}\, \mathrm{d}\Omega, \\ b(p, q) &= \int_\Omega \frac{\boldsymbol{K}}{\mu_f} \nabla p \cdot \nabla q\, \mathrm{d}\Omega. \end{aligned}$$

The initial condition is given by

$$\left(\frac{1}{M} p(0) + \alpha \nabla \cdot \boldsymbol{u}(0), q\right) = 0, \quad \forall\ q \in L_2(\Omega). \tag{12}$$

For the spatial discretization, we use a stabilized linear finite element method [19]. The stabilization proposed in that work was based on adding an artificial term to the flow equation with the purpose of eliminating the non-physical oscillations that the pressure field often exhibits when linear finite element methods are used to approximate both displacement and pressure unknowns. For this stabilized finite element method, discrete inf-sup stability conditions and convergence results were recently derived in [20]. We have chosen this discretization because of its simplicity, good monotonicity properties and rigorous convergence results. For time discretization, we consider a backward-Euler scheme.

Let $\mathcal{T}_h$ denote a triangulation of Ω satisfying the usual admissibility assumptions. Defining the discrete spaces as

$$\begin{aligned} \boldsymbol{V}_h &= \{\boldsymbol{u}_h \in (H^1(\Omega))^n \mid \forall T \in \mathcal{T}_h, \boldsymbol{u}_{h|T} \in \mathbb{P}_1^n,\ \boldsymbol{u}_h|_{\Gamma_c} = \boldsymbol{0}\}, \\ Q_h &= \{p_h \in H^1(\Omega) \mid \forall T \in \mathcal{T}_h, p_{h|T} \in \mathbb{P}_1,\ p_h|_{\Gamma_t} = 0\}, \end{aligned}$$

where $\mathbb{P}_1$ denotes the space of scalar piecewise linear functions on $\mathcal{T}_h$, the fully discretized scheme at time $t_m, m = 1, 2, \ldots$, can be written as the following:

find $(\boldsymbol{u}_h^m, p_h^m) \in \boldsymbol{V}_h \times Q_h$ such that

$$a(\boldsymbol{u}_h^m, \boldsymbol{v}_h) - \alpha(p_h^m, \operatorname{div} \boldsymbol{v}_h) = (\rho \boldsymbol{g}, \boldsymbol{v}_h), \quad \forall\ \boldsymbol{v}_h \in \boldsymbol{V}_h, \tag{13}$$

$$\alpha(\operatorname{div} \bar{\partial}_t \boldsymbol{u}_h^m, q_h) + \frac{1}{M}(\bar{\partial}_t p_h^m, q_h) + b(p_h^m, q_h) + c(\bar{\partial}_t p_h^m, q_h) = (f_h^m, q_h) + (\boldsymbol{K}\mu_f^{-1}\rho_f \boldsymbol{g}, \nabla q_h), \quad \forall\ q_h \in Q_h, \tag{14}$$

where $\bar{\partial}_t \boldsymbol{u}_h^m := (\boldsymbol{u}_h^m - \boldsymbol{u}_h^{m-1})/\tau$, $\bar{\partial}_t p_h^m := (p_h^m - p_h^{m-1})/\tau$, and the stabilization term is defined as

$$c(p_h, q_h) = \sum_{T \in \mathcal{T}_h} h_T^2 \int_T C_T (\nabla p_h \cdot \nabla q_h)\, \mathrm{d}\Omega,$$

where C_T is a constant independent of the space and time discretization parameters. Following [19], we fix the stabilization parameter as $C_T = (4(\lambda + 2G))^{-1}$, which was observed as optimal at least for one-dimensional problems. Notice that the stabilization term is, essentially, the time derivative of a diffusion operator multiplied by a stabilization parameter.

Thus, a linear system $\mathcal{A}x = b$ must be solved in each time step, where matrix $\mathcal{A}$ is a 2×2 block symmetric indefinite matrix of the form

$$\mathcal{A} = \begin{bmatrix} A & B^T \\ B & -C \end{bmatrix}, \tag{15}$$

with matrices A and C both symmetric and positive definite.

3. Fixed-stress split algorithm

115 In this section we describe the fixed-stress split algorithm and we explain how it can be interpreted mathematically. Then, we propose a class of smoothers based on this method.

3.1. The fixed-stress split algorithm

The fixed-stress split scheme for solving poroelasticity problem is an iterative method in which the flow problem is solved first supposing a constant volumetric mean total stress, and once the flow problem is solved, the elasticity problem is

then exactly solved. The volumetric mean total stress is defined as the mean of the trace of the total stress tensor, that is $\sigma_v = \mathrm{tr}(\boldsymbol{\sigma})/3$, and it is related to the volumetric strain $\varepsilon_v = \mathrm{tr}(\varepsilon)$ as

$$\sigma_v = K_b \varepsilon_v - \alpha p.$$

By using this relation, we write the flow equation in terms of the volumetric mean total stress instead of the volumetric strain,

$$\left(\frac{1}{M} + \frac{\alpha^2}{K_b}\right)\frac{\partial p}{\partial t} + \frac{\alpha}{K_b}\frac{\partial \sigma_v}{\partial t} - \nabla \cdot \left(\frac{1}{\mu_f}\boldsymbol{K}\left(\nabla p - \rho_f \boldsymbol{g}\right)\right) = f. \tag{16}$$

The fixed-stress split scheme is based on solving the flow equation (16) considering that the term $(\alpha/K_b)\partial\sigma_v/\partial t$ is known. In the discrete case, this is equivalent to an iterative method based on the splitting of matrix $\mathcal{A} = \mathcal{M}_A - \mathcal{N}_A$ as

$$\begin{bmatrix} A & B^T \\ B & -C \end{bmatrix} = \begin{bmatrix} A & B^T \\ 0 & -C + \frac{\alpha^2}{K_b} M_p \end{bmatrix} - \begin{bmatrix} 0 & 0 \\ -B & \frac{\alpha^2}{K_b} M_p \end{bmatrix}, \tag{17}$$

where M_p is the mass matrix. Notice that matrix $\mathcal{M}_A$ can be interpreted as an block-upper-triangular preconditioner where the Schur complement with respect to A, $-(C + BA^{-1}B^T)$ has been approximated by the matrix $S = -C + (\alpha^2/K_b)M_p$. As the discretization considered here satisfies a discrete inf-sup condition, mass matrix M_p is spectrally equivalent to $-BA^{-1}B^T$. This yields that $\mathcal{M}_A$ is an efficient preconditioner [13].

3.2. Smoothers based on the fixed-stress split method

We now present two physics-based type smoothers related to the splitting algorithm described above. In the multigrid context, it seems natural to consider as relaxation procedure an operator based on $\mathcal{M}_A$ replacing the two diagonal block matrices by suitable smoothers. This means to consider relaxations as

$$\widetilde{\mathcal{M}}_A = \begin{bmatrix} M_A & B^T \\ 0 & M_S \end{bmatrix},$$

with M_A and M_S suitable smoothers for operators A and S respectively. In this work, we mainly consider two relaxations of this type. The first smoother

is denoted as $\widetilde{\mathcal{M}}_{A,T1}$, and it is based on a symmetric Gauss-Seidel iteration for A; i.e.,

$$M_A = (D_A + L_A)D_A^{-1}(D_A + U_A),$$

where D_A, L_A and U_A are, respectively, the diagonal, the strict lower, and the strict upper parts of A; and on a symmetric Gauss-Seidel iteration for $S = -C + (\alpha^2/K_b)M_p$. Of course, other relaxation schemes for A and S can be considered, such as a red-black Gauss-Seidel method, etc.

The second relaxation procedure considered here is based on the smoother

$$M_{A,2} = M_A(2M_A - A)^{-1}M_A,$$

for the displacements and on a symmetric Gauss-Seidel iteration for $S = -C + (\alpha^2/K_b)M_p$. Smoother $M_{A,2}$ corresponds to two iterations of the symmetric Gauss-Seidel iteration as it can be seen from the relation $I - M_{A,2}^{-1}A = (I - M_A^{-1}A)^2$. We denote this smoother as $\widetilde{\mathcal{M}}_{A,T2}$.

In this work, we also consider smoothers based on a diagonal inexact version of the fixed-stress split scheme, that is,

$$\widetilde{\mathcal{M}}_A = \begin{bmatrix} M_A & 0 \\ 0 & M_S \end{bmatrix},$$

where again M_A and M_S are suitable smoothers for A and $S = -C+(\alpha^2/K_b)M_p$, respectively. This kind of smoothers can have some appeal on parallel computers, since the relaxation of the mechanics and flow parts can be executed in parallel. In particular, we consider a smoother based on two iterations of the symmetric Gauss-Seidel method for displacements, and one iteration of the symmetric Gauss-Seidel method for S. We denote it in this work as $\widetilde{\mathcal{M}}_{A,D2}$.

Remark. Notice that the proposed smoothers based on the fixed-stress split method can be easily adapted to be applied to other different discretizations of the problem as mixed finite-elements or finite volume schemes, for example.

3.3. Local Fourier analysis for the fixed-stress split smoothers

This section is devoted to the study of the proposed fixed-stress split smoothers by the local Fourier analysis technique. A smoothing analysis to show how effi-

ciently these relaxations annihilate the high-frequency components of the error is performed.

3.3.1. Basis of LFA

We first briefly introduce the basic notation and facts which have to be assumed to perform the local Fourier analysis. It is assumed that all discrete operators have constant coefficients and are defined on an infinite grid Ω_h, neglecting the effect of boundary conditions. In this way, all occurring multigrid components, the discrete approximation and its corresponding error can be represented by formal linear combinations of the so-called Fourier modes, defined as $\varphi_h(\boldsymbol{\theta}, \mathbf{x}) = e^{\imath \boldsymbol{\theta} \cdot \mathbf{x}/\mathbf{h}}$, where $\boldsymbol{\theta} \in \boldsymbol{\Theta} := (-\pi, \pi]^2$. These grid-functions result then to be "eigenfunctions" of the smoothing operator and the corresponding "eigenvalues" give rise to the so-called Fourier symbol of the relaxation procedure.

We distinguish high- and low-frequency components on Ω_h, since we are interested in the behavior of the smoother for the high-frequency Fourier modes. The classification of "high" and "low" is done with respect to the coarse grid, which in this case is built by using standard coarsening, that is, the step size is double in each direction on the coarse grid, which is denoted by Ω_{2h}. Then, low-frequencies are defined as $\boldsymbol{\Theta}_2 = (-\pi/2, \pi/2]^2$ and therefore the high-frequencies are given by $\boldsymbol{\Theta} \backslash \boldsymbol{\Theta}_2$.

One can perform a local Fourier smoothing analysis by considering the corresponding Fourier domain representation or the Fourier symbol of the smoothing operator $\widetilde{S}_h(\boldsymbol{\theta})$ on the high frequencies. This gives rise to the computation of the so-called smoothing factor, which is defined as

$$\mu = \sup_{\boldsymbol{\Theta} \backslash (-\pi/2, \pi/2]^2} \rho(\widetilde{S}_h(\boldsymbol{\theta})). \tag{18}$$

3.3.2. Smoothing analysis of the fixed-stress split smoother

Next, we want to analyze the smoothing properties of the proposed class of smoothers based on the fixed-stress split method. We fix a uniform right

triangular grid, for example, but the analysis can be performed on any regular triangular grid.

Figure 1 presents the spectra of (a) $I - \mathcal{M}_A^{-1}\mathcal{A}$ and (b) $I - \widetilde{\mathcal{M}}_{A,T1}^{-1}\mathcal{A}$ respectively. It can be observed from Figure 1 (a) that we have good convergence properties for the fixed-stress method, but one has to solve the mechanics and flow parts on each iteration. In the right picture we see that the inexact version of this algorithm, although still converging, is not a good option, as we have eigenvalues close to one.

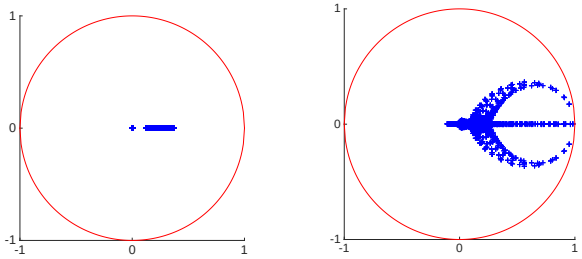

(a) (b)

Figure 1: Spectral pictures of (a) $I - \mathcal{M}_A^{-1}\mathcal{A}$, and (b) $I - \widetilde{\mathcal{M}}_{A,T1}^{-1}\mathcal{A}$

If we restrict the spectrum to the high frequencies, however, it is observed in Figure 2(a) that $\widetilde{\mathcal{M}}_{A,T1}^{-1}$ is an excellent smoother within a multigrid framework. Similar results are shown for $\widetilde{\mathcal{M}}_{A,T2}^{-1}$ in Figure 2(b). For completeness, we also display in Figure 2(c) the spectrum of the diagonal version of the inexact method restricted to the high frequencies. Although it provides worse results than the previous ones, it could be interesting to consider this smoother due to its excellent parallelization properties.

4. Multigrid method

In this section we consider the components involved in the coarse-grid correction part of the multigrid algorithm, and we analyze the performance of the

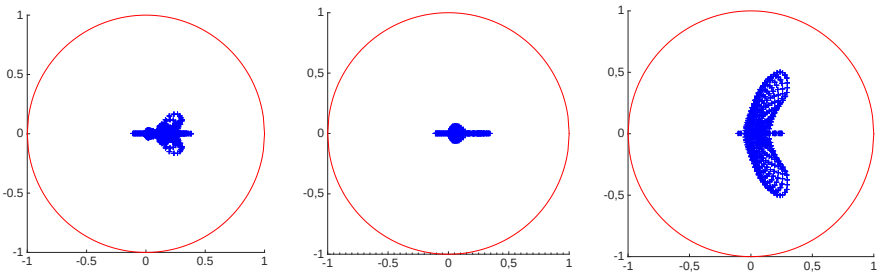

(a) (b) (c)

Figure 2: Spectral pictures of (a) $I - \widetilde{\mathcal{M}}_{A,T1}^{-1}\mathcal{A}$, (b) $I - \widetilde{\mathcal{M}}_{A,T2}^{-1}\mathcal{A}$, and (c) $I - \widetilde{\mathcal{M}}_{A,D2}^{-1}\mathcal{A}$ restricted to the high-frequencies.

resulting multigrid method by using a two-grid local Fourier analysis. This analysis will allow us to derive the corresponding asymptotic convergence factors of the algorithm.

4.1. Multigrid components

We propose a monolithic geometric multigrid method for solving the quasi-static Biot's model for soil consolidation. The previously introduced class of smothers based on the fixed-stress split algorithm is considered for the relaxation process within the proposed multigrid method. Regarding the coarse-grid correction part of the algorithm, a standard coarsening strategy is chosen to construct the grid-hierarchy, which will be composed of regular triangular grids. Standard seven-point restriction and interpolation operators are used for the transfer of information between the meshes.

4.2. Two-grid local Fourier analysis

The behavior of the multigrid method can be analyzed by evaluating the error reduction associated with each particular multigrid component on the Fourier modes previously defined. In the transition from the fine to the coarse grid each low-frequency $\boldsymbol{\theta}^{00} \in \boldsymbol{\Theta}_2$ is coupled with three high frequencies, giving rise to the so-called spaces of $2h$-harmonics, $\mathcal{F}^4(\boldsymbol{\theta}^{00}) = span\{\varphi_h(\boldsymbol{\theta}^{\alpha_1\alpha_2}, x) | \alpha_1, \alpha_2 \in$

$\{0,1\}\}$, with $\boldsymbol{\theta}^{\alpha_1\alpha_2} = \boldsymbol{\theta}^{00} - (\alpha_1 \text{sign}(\theta_1^{00})\pi, \alpha_2 \text{sign}(\theta_2^{00})\pi)$. Then, the coarse–grid correction operator $(I_h - I_{2h}^h L_{2h}^{-1} I_h^{2h} L_h)$, composed of the discrete operators on the fine and coarse grids, L_h and L_{2h}, respectively, and the inter–grid transfer operators: restriction, I_h^{2h} and prolongation I_{2h}^h, as well as the smoother S_h, leave these subspaces invariant. This implies that the two-grid method $M_h^{2h} = S_h^{n_2}(I_h - I_{2h}^h L_{2h}^{-1} I_h^{2h} L_h) S_h^{n_1}$, also does, and therefore M_h^{2h} is equivalent to a block–diagonal matrix consisting of blocks denoted by $\widetilde{M}_h^{2h}(\boldsymbol{\theta}^{00}) = M_h^{2h}|_{\mathcal{F}^4(\boldsymbol{\theta}^{00})}$. In this way, one can determine the spectral radius $\rho(M_h^{2h})$ by calculating the spectral radius of these smaller matrices, that is:

$$\rho = \rho(M_h^{2h}) = \sup_{\boldsymbol{\theta}^{00} \in \boldsymbol{\Theta}_2} \rho(\widetilde{M}_h^{2h}(\boldsymbol{\theta}^{00})). \tag{19}$$

The two-grid analysis is the basis for the classical asymptotic multigrid convergence estimates, and the spectral radius of the two–grid operator, $\rho(M_h^{2h})$, indicates the asymptotic convergence factor of the two-grid method.

4.2.1. Local Fourier analysis results

Next, we present some results from the two-grid analysis previously introduced. For these results, the material parameters are given by $E = 10^4, \nu = 0.2$, being E and ν the Young's modulus and the Poisson ratio, respectively. From these values, the Lamé coefficients can be obtained by the following formulas

$$\lambda = \frac{\nu E}{(1+\nu)(1-2\nu)}, \quad G = \frac{E}{2(1+\nu)}.$$

Moreover, we consider a diagonal permeability tensor $\mathbf{K} = k\mathbf{I}$ with constant k.

In order to show that the local Fourier analysis gives very accurate predictions of the real asymptotic convergence factor of the multigrid method, in Table 1 we compare the two-grid convergence factor ρ predicted by LFA with the asymptotic convergence factor ρ_h experimentally computed by using a $W-$cycle. For these tests we consider a uniform right triangular grid and also a regular equilateral triangular grid. However, the local Fourier analysis presented can be performed on any regular triangular grid. We display the results for different numbers of smoothing steps $n = n_1 + n_2$ and for a fixed value of parameter k,

	n	$\mathcal{M}_{A,T1}$	$\mathcal{M}_{A,T2}$	$\mathcal{M}_{A,D2}$
Right	1	0.45 (0.46)	0.28 (0.29)	0.28 (0.29)
	2	0.28 (0.29)	0.16 (0.17)	0.16 (0.16)
	3	0.20 (0.21)	0.12 (0.12)	0.12 (0.12)
	4	0.16 (0.17)	0.08 (0.09)	0.08 (0.09)
Equilateral	1	0.35 (0.35)	0.17 (0.17)	0.17 (0.17)
	2	0.13 (0.14)	0.05 (0.06)	0.05 (0.06)
	3	0.08 (0.08)	0.03 (0.04)	0.03 (0.04)
	4	0.05 (0.06)	0.02 (0.03)	0.02 (0.03)

Table 1: Comparison between the two-grid analysis convergence factors predicted by LFA ρ and the experimentally computed asymptotic convergence factors ρ_h (between brackets), for different numbers of smoothing steps n, two different regular triangular grids (right and equilateral) and $k = 10^{-3}$.

that is $k = 10^{-3}$. From the table we can observe a very good agreement between the predicted values and the experimentally obtained ones, which makes the LFA a very useful tool for the study of the convergence of the multigrid method based on the fixed-stress split relaxation.

Also, we observe that the diagonal version of $\mathcal{M}_{A,T2}$, that is, smoother $\mathcal{M}_{A,D2}$ provides similar results, resulting in a very appealing alternative due to its parallelizable properties.

Robustness with respect to the permeability. Next, we want to show the robustness of the proposed class of smoothers with respect to the permeability. For this purpose, in Table 2 we display the two-grid convergence factors provided by LFA for different values of the permeability k and an increasing number of smoothing steps n from $n = 1$ to $n = 4$. We can observe that the triangular smoothers provide a very robust behavior for different values of the permeability, and that the obtained asymptotic convergence rates are around 0.1 with only two smoothing steps. The diagonal version also provides very good results identically to the corresponding triangular version.

		Right			Equilateral		
	$n \setminus k$	1	10^{-3}	10^{-6}	1	10^{-3}	10^{-6}
$\mathcal{M}_{A,T1}$	1	0.45	0.45	0.45	0.35	0.35	0.35
	2	0.28	0.28	0.28	0.13	0.13	0.13
	3	0.20	0.20	0.20	0.08	0.08	0.08
	4	0.16	0.16	0.16	0.05	0.05	0.05
$\mathcal{M}_{A,T2}$	1	0.28	0.28	0.28	0.17	0.17	0.17
	2	0.16	0.16	0.16	0.05	0.05	0.05
	3	0.12	0.12	0.12	0.03	0.03	0.03
	4	0.08	0.08	0.08	0.02	0.02	0.02
$\mathcal{M}_{A,D2}$	1	0.28	0.28	0.28	0.17	0.17	0.17
	2	0.16	0.16	0.16	0.05	0.05	0.05
	3	0.12	0.12	0.12	0.03	0.03	0.03
	4	0.08	0.08	0.08	0.02	0.02	0.02

Table 2: Two-grid analysis convergence factors predicted by LFA for different values of parameter k, by using different numbers of smoothing steps n, and considering two different uniform triangular grids (right and equilateral).

4.3. Multigrid on semi-structured grids

To deal with irregular domains, it is very common to apply a regular refinement process to an unstructured input grid to obtain a particular hierarchy of globally unstructured grids, but with structured patches. The basic idea to construct the hierarchy of semi-structured meshes is to begin with a purely unstructured grid, which will be our coarsest mesh, and to apply several steps of regular refinement to each element. This is done by dividing each triangle into four congruent triangles, connecting the midpoints of their edges (see Figure 3), and so forth until the mesh has the desired meshwidth to handle the fine scale features and to approximate accurately the solution of the problem. The initial unstructured mesh is chosen however to adequately represent the geometry of the domain, taking into account the large scale structure, that is, the shape and

the material properties.

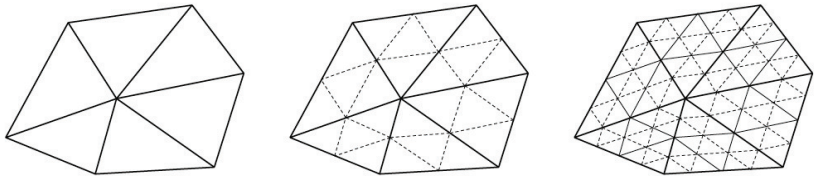

Figure 3: Coarsest unstructured grid and the semi-structured meshes obtained after one and two regular refinement steps.

The semi-structured grid framework serves as the basis of an efficient implementation in terms of memory consumption, parallelization and performance of the proposed solver. First, the regularity of the structured regions makes that transfer operations between grids can be defined geometrically, allowing a straightforward implementation of a geometric multigrid algorithm. Moreover, explicit assembly of the global matrix is not necessary in the structured patches of the grid and then the discrete operator can be implemented using a stencil-based data structure [21].

5. Numerical results

In this section we illustrate the good convergence properties of the proposed multigrid based on the fixed-stress split smoothers through two numerical experiments. For the following tests we have considered the diagonal version of the fixed-stress split smoother, that is $\mathcal{M}_{A,D2}$, since it provides convergence rates similar to the triangular version and because of its parallelizable properties.

5.1. Poroelastic footing problem

For the first numerical experiment we deal with the so-called poroelasticity footing problem [22], which is solved on the computational domain $\Omega = [0,1] \times [0,\sqrt{3}/2]$, represented in Figure 4 (a). The base of this domain is assumed to be rigid, whereas a uniform load of intensity $\sigma_0 = 10^4 \mathrm{N/m}^2$ is applied in a strip of

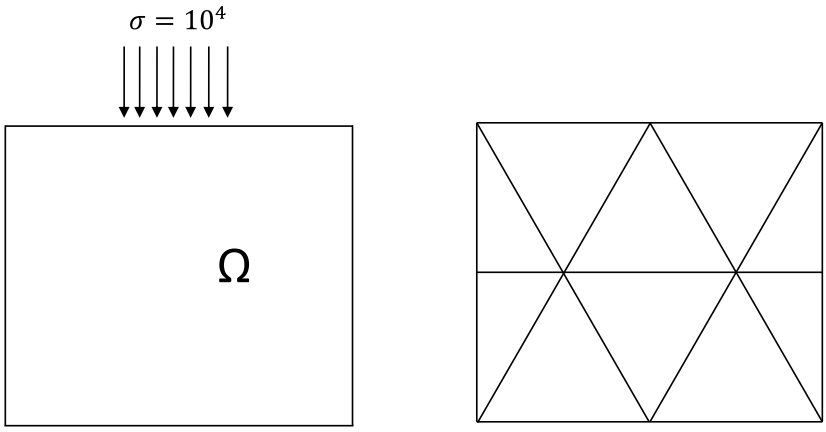

Figure 4: (a) Computational domain and boundary conditions for the poroelastic footing problem. (b) Coarsest grid in the hierarchy of semi-structured meshes.

length 0.4, at the centered part of the upper boundary. Except the upper part, which is assumed free to drain, the rest of the boundary is impermeable. More concretely, we can split the boundary $\Gamma = \partial\Omega$ into three different parts given by

$$\begin{aligned}
\Gamma_{t,1} &= \{(x,y) \in \Gamma \,|\, y = \sqrt{3}/2,\ 0.3 \leq x \leq 0.7\}, \\
\Gamma_{t,2} &= \{(x,y) \in \Gamma \,|\, y = \sqrt{3}/2,\ 0 < x < 0.3 \text{ or } 0.7 < x < 1\}, \\
\Gamma_{c} &= \Gamma \backslash \{\Gamma_{t,1} \cup \Gamma_{t,2}\}.
\end{aligned}$$

Then, the imposed boundary conditions are as follows,

$$\mathbf{u} = \mathbf{0} \ \text{ and } \ \nabla p \cdot \mathbf{n} = 0 \ \text{ on } \ \Gamma_c,$$

$$\boldsymbol{\sigma}'\mathbf{n} = \mathbf{t} \ \text{ on } \ \Gamma_{t,1}, \quad \boldsymbol{\sigma}'\mathbf{n} = \mathbf{0} \ \text{ on } \ \Gamma_{t,2}, \quad p = 0 \ \text{ on } \ \Gamma_{t,1} \cup \Gamma_{t,2},$$

where $\mathbf{t} = (0, -\sigma_0)^t$ gives the traction applied on the top boundary part.

Regarding the material parameters, we are going to study three different cases: one corresponding to an homogeneous porous medium, one corresponding to two layers with different physical parameters and one corresponding to random heterogeneous materials.

5.1.1. Homogeneous porous medium

In this first case, the material properties of the porous medium are given by $E = 3 \times 10^4$ and $\nu = 0.2$. The viscosity of the fluid is considered as $\mu_f = 10^{-3}$ and we will consider different values of parameter k defining the diagonal permeability tensor $\mathbf{K} = k\mathbf{I}$.

For the application of the proposed multigrid method, we need to define a hierarchy of grids. This is done by choosing as the coarsest triangulation the one depicted in Figure 4 (b), which is composed of 10 triangles, and to apply several iterations of a regular refinement process to each element until achieving a target grid with the desired fine scale to approximate the solution of the problem. Once the hierarchy of grids is built, we can apply the geometric multigrid method based on the fixed-stress split relaxation to solve the poroelastic footing problem. To do this, we will consider an $F-$ cycle with two pre-smoothing steps and one post-smoothing step. We are interested in the behavior of the algorithm for different values of the physical parameters. Thus, in Table 3, we show the numbers of iterations that are needed to reduce the initial residual in a factor of 10^{-10} when different finest grids are considered and for different values of the permeability, including very small ones, which are representative of real applications. We can observe that the performance of the solver is independent of the space discretization parameter and also is very robust with respect to the permeability value.

5.1.2. Two-layered porous medium

Secondly, we want to investigate the performance of the proposed multigrid method when a two-layered porous medium is considered. The computational domain is the same as given in Figure 4 (a), which is assumed to be composed of two equally sized layers of porous material with different physical properties. The values of the material parameters on each layer are given in Figure 5.

We solve such poroelastic problem by applying the same multigrid method used for the homogeneous porous media test. Notice that the only difference is that the parameter appearing in the fixed-stress split smoother will be different

$\tau k/\mu_f$	6 levels	7 levels	8 levels	9 levels	10 levels
10^{-2}	11	11	11	11	11
10^{-4}	11	11	11	11	11
10^{-6}	11	11	11	11	11
10^{-8}	10	11	11	11	11
10^{-10}	12	11	10	10	11
10^{-12}	12	12	12	12	12

Table 3: Number of iterations necessary to reduce the initial residual in a factor of 10^{-10} for different physical parameters and different fine grids obtained by using different numbers of refinement levels.

from one layer to another, since it depends on the Lamé coefficients λ and G. In Figure 6 we show the history of the convergence of the proposed multigrid method for different target grids obtained by applying different numbers of refinement levels. The reduction of the maximum residual is plotted against the number of iterations, and we observe an independent performance of the algorithm with respect to the space discretization parameter. Moreover, we can see that in all cases around ten iterations are enough to reduce the initial maximum residual in a factor of 10^{-10}.

5.1.3. Random heterogeneous materials

In this third case, we study the robustness of the multigrid method in heterogeneous random media. The permeability is modeled as a lognormal random field, i.e. $\log K$ is a zero-mean Gaussian random field. It is well known that a lognormal random field may accurately represent the permeability of a heterogeneous porous medium [23]. To generate samples of the Gaussian random $\log K$, we have used the covariance function

$$C(r) = \sigma_c^2 \exp\left(-\frac{r}{\lambda_c}\right)$$

characterized by the correlation length λ_c and the variance σ_c^2, and where r is the distance between two points. In the numerical experiment, we use two different

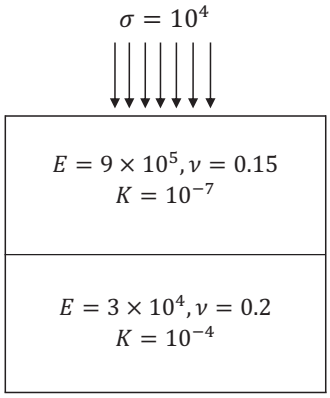

Figure 5: Computational domain and material properties for the two-layered poroelastic footing problem.

set of parameters, $(\lambda_c, \sigma_c) = (0.3, 1)$ and $(\lambda_c, \sigma_c) = (0.1, 3)$. As an example, in Figure 7, we present a possible sample of the logarithm of the permeability field, $\log K$, using each of the two sets of parameters. It can be observed that very large fluctuations happen in the permeability field for the case with $\sigma_c = 3$. Moreover, it is assumed that the Young's modulus as well as the Poisson ratio are independent Gaussian random variables.

Notice that the parameter involved in the fixed-stress split smoother depends on the mechanical parameters of the medium. This yields that in this experiment such parameter must be calculated on each element. All the random parameters defined on the finest grid are restricted to each coarse grid of the hierarchy as the average value of the neighbouring grid points.

The performance of the proposed multigrid method based on the fixed-stress split smoother for this experiment with random heterogeneous materials is very satisfactory as in the previous cases. We have computed an average of the convergence factors obtained after 50 realizations of the random field, and a convergence rate of 0.11 is obtained in the case of $(\lambda_c, \sigma_c) = (0.3, 1)$. When $(\lambda_c, \sigma_c) = (0.1, 3)$, however, the very large fluctuations of the permeability field cause a slight deterioration of the convergence of the multigrid method, and

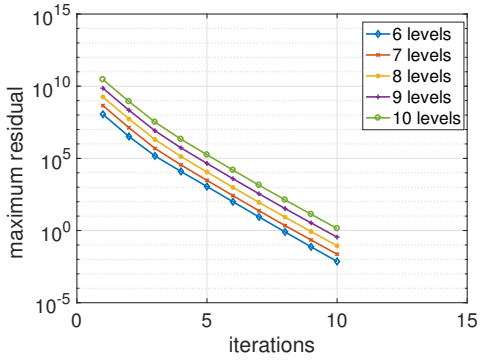

Figure 6: History of the convergence of the multigrid algorithm based on the fixed-stress split relaxation for the two-layered poroelastic footing problem for different numbers of refinement levels.

the obtained mean convergence factor is around 0.33. Notice that even using a standard coarse-grid correction operator the performance of the multigrid method is still satisfactory.

5.2. Poroelastic problem on a cylindrical shell

As the second numerical experiment, we consider a poroelastic problem on a cylindrical shell of deformable porous material in which a uniform load is applied at the inner boundary. In particular, a fixed pressure $p = 1$ is imposed in the inner surface of the cylinder, which produces a uniform load described by $\boldsymbol{\sigma}\mathbf{n} = (\cos\theta, \sin\theta)$. The outer boundary, which is impermeable, is constrained by a rigid body. More concretely, the considered boundary conditions are depicted in Figure 8, where also the computational domain is shown. The considered physical parameters are as stated in the previous numerical experiment, but in this case the permeability is fixed to be $k = 10^{-6}$.

In order to apply the fixed-stress split relaxation based multigrid, a hierarchy of grids must be defined. For the unstructured coarsest grid, we have chosen the triangulation shown in Figure 9 (a), which is composed of 18 quite regular triangles. A regular refinement process is applied to this triangulation, giving rise to a hierarchy of semi-structured meshes. Due to the curvature of the

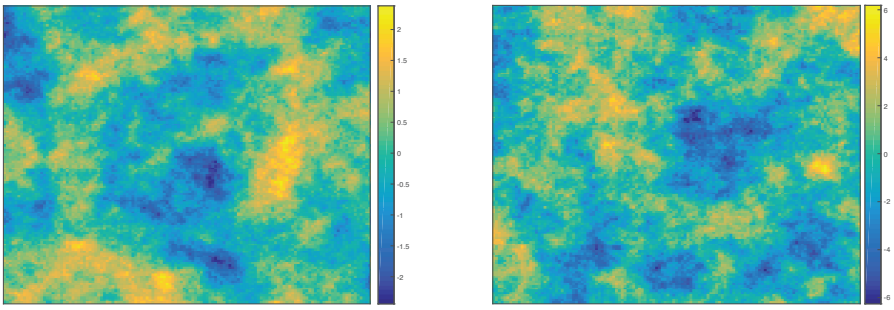

(a) (b)

Figure 7: Examples of the logarithm of the permeability field (a) using parameters $(\lambda_c, \sigma_c) = (0.3, 1)$ (b) using parameters $(\lambda_c, \sigma_c) = (0.1, 3)$

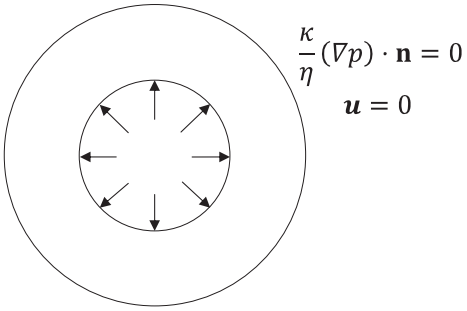

Figure 8: Computational domain and boundary conditions for the poroelastic problem on a cylindrical shell.

boundary, the refinement procedure is performed in the way that the more we refine the more the grid approximates the real boundary of the domain. More concretely, the refinement of a triangle of the coarsest grid which has two vertices on the boundary is performed in the following way: the new boundary point is taken as the intersection of the perpendicular bisector of the edge with the corresponding boundary arc. For instance, the grid obtained after four refinement levels is depicted in Figure 9 (b) as an example, where it can be seen how well the refined grid approximates the real boundary of the domain.

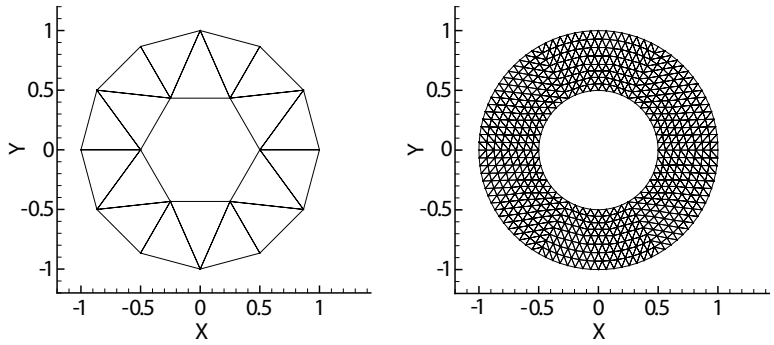

Figure 9: (a) Coarsest grid in the hierarchy of semi-structured meshes, and (b) grid obtained after four regular refinement levels.

Once obtained the hierarchy of meshes, we apply the proposed geometric multigrid method based on the fixed-stress split smoother to solve the poroelastic problem on the cylindrical shell. In Figure 10 we show the history of the convergence for different target grids obtained by applying different numbers of refinement levels, and by using an $F-$cycle with two pre- and one post-smoothing steps. We can observe that we obtain a convergence independent of the space discretization parameter and that few iterations are enough to obtain the desired convergence.

Remark. Given the thinly-layered nature of many geologic formations, the use of meshes with thin elements with very large aspect ratios can be appealing in reservoir simulations. Under such challenging test-conditions the convergence of multigrid methods based on point-wise smoothers, as those considered here, is expected to deteriorate as the grid becomes more anisotropic, and then appropriate block-wise smoothers or semi-coarsening strategies may be required. For example, in the experiment with smoothly random heterogeneous materials, if a thin rectangular domain with an aspect ratio of 10:1 is considered as our domain, triangulated with two right triangles as the coarsest grid, we can observe a deterioration of the convergence of the proposed multigrid method based on

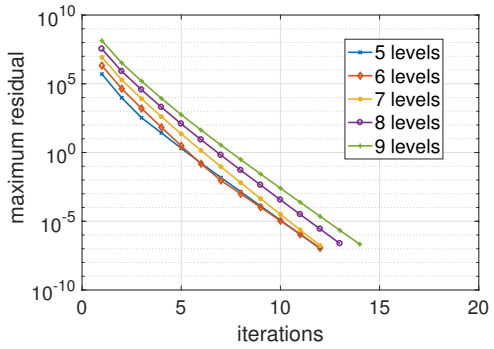

Figure 10: History of the convergence of the fixed-stress split smoother based multigrid method for the cylindrical shell poroelastic problem for different numbers of refinement levels.

the fixed-stress split method from 0.1 to a convergence rate of 0.9. To overcome this difficulty, we have implemented a line-wise version of the fixed-stress split method which consists to simultaneously update all the unknowns located at the line where the strong coupling occurs. By using this smoother, the convergence rate that we obtain with the considered $F(2,1)$-cycle is improved to 0.03.

6. Conclusions

In this paper we have proposed a new smoother within a multigrid method for solving the Biot's consolidation problem. This relaxation is based on the well-known fixed-stress iterative coupling scheme, whose parameters only depend on the physics of the problem. The proposed monolithic multigrid method has the advantage of being a fully coupled method which decouples the flow and geomechanics problems in the smoothing part of the algorithm. It has been shown that the performance of the algorithm is very satisfactory independently of the values of the physical parameters, and its application to different problems in semi-structured triangular grids makes it suitable for dealing with problems in reasonably complex domains.

Acknowledgements

The work of Francisco J. Gaspar is supported by the European Union's Horizon 2020 research and innovation programme under the Marie Sklodowska-Curie grant agreement NO 705402, POROSOS. The research of Carmen Rodrigo is supported in part by the Spanish project FEDER /MCYT MTM2016-75139-R and the DGA (Grupo consolidado PDIE). We thank Prashant Kumar for his help and discussion with the Matlab code for the heterogeneous test.

References

[1] L. Bergamaschi, M. Ferronato, G. Gambolati, Novel preconditioners for the iterative solution to FE-discretized coupled consolidation equations, Computer Methods in Applied Mechanics and Engineering 196 (25) (2007) 2647 – 2656.

[2] M. Ferronato, L. Bergamaschi, , G. Gambolati, Performance and robustness of block constraint preconditioners in finite element coupled consolidation problems, International Journal for Numerical Methods in Engineering 81 (2010) 381 – 402.

[3] F. J. Gaspar, F. J. Lisbona, C. Oosterlee, R. Wienands, A systematic comparison of coupled and distributive smoothing in multigrid for the poroelasticity system, Numerical Linear Algebra with Applications 11 (2004) 93–113.

[4] P. Luo, C. Rodrigo, F. J. Gaspar, C. W. Oosterlee, On an Uzawa smoother in multigrid for poroelasticity equations, Numerical Linear Algebra with Applications 24 (1), e2074 nla.2074. doi:10.1002/nla.2074.

[5] J. Kim, H. A. Tchelepi, R. Juanes, Stability, accuracy and efficiency of sequential methods for coupled flow and geomechanics, In the SPE Reservoir Simulation Symposium, Houston, Texas, 2009 SPE 119084.

[6] J. Kim, Sequential methods for coupled geomechanics and multiphase flow, Stanford University, 2010.

[7] J. Kim, H. A. Tchelepi, R. Juanes, Stability and convergence of sequential methods for coupled flow and geomechanics: fixed-stress and fixed-strain splits, Computer Methods in Applied Mechanics and Engineering 200 (13-16) (2011) 1591 – 1606.

[8] A. Mikelic, M. F. Wheeler, Convergence of iterative coupling for coupled flow and geomechanics, Computational Geosciences (17) (2013) 455–461.

[9] J. Both, M. Borregales, J. Nordbotten, K. Kumar, F. Radu, Robust fixed stress splitting for Biot's equations in heterogeneous media, Applied Mathematics Letters 68 (2017) 101 – 108.

[10] T. Almani, K. Kumar, A. Dogru, G. Singh, M. Wheeler, Convergence analysis of multirate fixed-stress split iterative schemes for coupling flow with geomechanics, Computer Methods in Applied Mechanics and Engineering 311 (1) (2016) 180 – 207.

[11] M. Bause, F. Radu, U. Kocher, Space-time finite element approximation of the Biot poroelasticity system with iterative coupling, Computer Methods in Applied Mechanics and Engineering 320 (2017) 745 – 768.

[12] N. Castelleto, J. A. White, H. A. Tchelepi, Accuracy and convergence properties of the fixed-stress iterative solution of two-way coupled poromechanics, International Journal for Numerical and Analytical Methods in Geomechanics 39 (2015) 1593 – 1618.

[13] J. A. White, N. Castelleto, H. A. Tchelepi, Block-partitioned solvers for coupled poromechanics: A unified framework, Computer Methods in Applied Mechanics and Engineering 303 (2016) 55–74.

[14] N. Castelleto, J. A. White, M. Ferronato, Scalable algorithms for three-field mixed finite element coupled poromechanics, Journal of Computational Physics 327 (2016) 894 – 918.

[15] H. F. Wang, Theory of linear poroelasticity with applications to geomechanics and hydrogeology., Princeton University Press., 2000.

[16] O. Coussy, Poromechanics, John Wiley & Sons, Ltd, 2004.

[17] M. A. Biot, General theory of three-dimensional consolidation, Journal of Applied Physics 12 (2) (1941) 155–164.

[18] M. A. Biot, Theory of elasticity and consolidation for a porous anisotropic solid, Journal of Applied Physics 26 (2) (1955) 182–185.

[19] G. Aguilar, F. Gaspar, F. Lisbona, C. Rodrigo, Numerical stabilization of Biot's consolidation model by a perturbation on the flow equation, International Journal for Numerical Methods in Engineering 75 (11) (2008) 1282–1300.

[20] C. Rodrigo, F. Gaspar, X. Hu, L. Zikatanov, Stability and monotonicity for some discretizations of the Biot's consolidation model, Computer Methods in Applied Mechanics and Engineering 298 (2016) 183–204.

[21] C. Rodrigo, F. J. Gaspar, F. J. Lisbona, Multigrid methods on semi-structured grids, Archives of Computational Methods in Engineering 19 (4) (2012) 499–538.

[22] M. A. Murad, A. F. D. Loula, On stability and convergence of finite element approximations of Biot's consolidation problem, International Journal for Numerical Methods in Engineering 37 (4) (1994) 645–667.

[23] R. A. Freeze, A stochastic-conceptual analysis of one-dimensional groundwater flow in nonuniform homogeneous media, Water Resources Research 11 (5) (1975) 725–741. doi:10.1029/WR011i005p00725.
URL http://dx.doi.org/10.1029/WR011i005p00725